Science Press

ARTICLE

In-situ Synthesis of Graphene/TiO$_2$ Nanocomposites via Microwave as Anode Materials for Li-ion Batteries

Yang Liangwei,   Chen Haoran,   Jin Xin,   Liu Wei,   Yu Xinmin,   Liu Junpeng,   Song Huanjun,   Li Xiaodong,   Yu Yi,   Wang Peng,   Zhang Baopeng

Research Institute of Aerospace Special Materials and Processing Technology, Beijing 100074, China

Abstract: Through the modified household microwave oven system, the graphene-based nanocomposites were in-situ and efficiently synthesized. Results show that the graphene nanosheets can be uniformly generated on the surface of the commercial anatase TiO$_2$ nanoparticles by microwave-assisted method in a few minutes (the minimum duration is 3 min) through the acute corona discharge of SiO$_2$/Si. The size of graphene nanosheet is about 50 nm, and few defects can be observed. The crystal structure of anatase TiO$_2$ remains due to the short production period and low synthesis temperature (600~700 °C). The excellent electrical conductivity of graphene can improve the Li ion diffusion and the electron transport, and decrease the contact resistance at the interface of electrode/ electrolyte. The as-prepared graphene/TiO$_2$ nanocomposite electrode shows a two-fold increase of capacity with good cycling stability under the condition of 1 C (170 mA·g^{-1}), compared with the traditional TiO$_2$ nanoparticles. The specific capacity gap of graphene/TiO$_2$ nanocomposite is substantially widened under different charge-discharge rates (1~5 C), compared with that of the commercial anatase TiO$_2$ nanoparticles.

Key words: graphene/TiO$_2$ nanocomposites; microwave-assisted; corona discharge; in-situ synthesis; Li-ion batteries

Graphene is a promising material because of its excellent electronic and mechanical properties, as well as large specific surface area, and good chemical stability[1]. Graphene-based nanocomposites have been widely investigated in the fields of energy, environment, and biomedical applications[2]. Various synthesis approaches have been proposed for graphene/nanoparticle (NP) composites. Commonly, NPs are designed to grow on the graphene oxide (GO) and then the graphene oxide is reduced, namely rGO[3]. The functional groups of GO and rGO, including hydroxyl and carboxylic groups, provide abundant nucleus sites. These functional groups interact with the deposited components, therefore controlling the size, morphology, and crystallinity of NPs[4]. Compared with GO, rGO has less functional groups and can form much larger NPs due to easy diffusion and recrystallization. Ni(OH)$_2$ nanocrystals synthesized on GO and rGO have different features because of different growth mechanisms. The advanced approach of graphene application is the graphene/NPs composites with graphene on NP surface. Chemical vapor deposition (CVD) technique has been widely employed to encapsulate NPs with graphene, which involves a carbon precursor gas flowing into a uniform heated chamber and then decomposing into carbon species on the vicinity of the heated surface for deposition of graphene nanosheets[5]. However, the synthesis procedure is relatively complex, the interaction of graphene sheets and NPs is poor, and the distribution of graphene and NPs is not uniform, which all restrict the application of graphene/NP composites.

A simple and efficient method for in-situ synthesis of graphene/TiO$_2$ (G/TiO$_2$) nanocomposites using a modified household microwave oven system is proposed in this research. In the modified microwave system, the carbon precursor flows into the chamber and decomposes into carbon species by acute corona discharge of SiO$_2$/Si. At the interface between atmosphere and commercial anatase TiO$_2$ NPs, these carbon species can nucleate and grow into graphene nanosheets in a few minutes (the minimum duration is 3 min). The size of graphene is about 50 nm, and few defects can be

observed. The distribution of graphene nanosheets on TiO_2 NPs is uniform due to the high frequency vibration of the TiO_2 NPs in the acute corona discharge process. Compared with CVD method, the anatase TiO_2 NPs can maintain the crystal structure due to the lower production temperature and shorter production period.

1 Experiment

A conventional household microwave oven with a frequency of 2.45 GHz was modified specifically for corona discharge process. Most area (70%) of a customized cylinder quartz boat was enclosed at both ends to avoid the spilling of TiO_2 NPs due to violent vibration during the reaction process. The commercial anatase TiO_2 NPs (~25 nm, 1~5 g) and some SiO_2/Si slices (~10 mm×10 mm×1 mm) with edges after cleaning were firstly put inside the quartz boat. Then the quartz boat was put into a quartz tube of modified household microwave oven under the argon flow condition (300~400 mL/min) to expel the residual air in the quartz tube. As the methane (30~50 mL/min) flowed into the oven system and the SiO_2/Si slices were exposed to the microwave irradiation, the continuous bright flash (corona discharge) occurred. After 3~5 min, the in-situ synthesis reaction was finished. As the oven system was naturally cooled down to room temperature, the graphene/TiO_2 nanocomposites could be collected.

Raman spectroscopy (Horiba Jobin Yvon LabRAM HR 800, 514.5 nm) was used to characterize the defect and quality of exfoliated graphene sheets. X-ray photoelectron spectroscope (XPS, Kratos Analytical Axis-Ultra spectrometer with Al Kα X-ray source) and X-ray diffraction (XRD, D/MAX-PC 2500, Cu Kα1) were used to investigate the quality of graphene film. Aberration corrected transmission electron microscopy (TEM, Titan Cubed Themis G2 300) was used to characterize the microstructure of G/TiO_2 nanocomposites.

The electrochemical properties of the G/TiO_2 nanocomposites and TiO_2 NPs as anode materials in lithium-ion batteries were evaluated through coin cells and pure Li foil as counter electrode. The coin cells were assembled in an argon-filled glovebox. To prepare the working electrodes, the mixture of active materials (G/TiO_2 nanocomposites or TiO_2 NPs), carbon black (Super-P), and poly(vinyl difluoride) (PVDF) at a mass ratio of 80:10:10 was pasted onto the pure

copper foil. The electrolyte consisted of 1 mol/L $LiPF_6$ and the mixed solution of ethylene carbonate (EC)/dimethyl carbonate (DMC)/diethyl carbonate (DEC) with mass ratio of 1:1:1. The coin cells were tested through galvanostatic charging-discharging experiments at different rates of 1~3 V vs. Li^+/Li.

2 Results and Discussion

2.1 In-situ synthesis of G/TiO_2 nanocomposites

Fig.1 shows the schematic diagram of synthesis of G/TiO_2 nanocomposites by the modified household microwave oven system. The appearances of the modified household microwave oven with a frequency of 2.45 GHz and the continuous bright flash (corona discharge) are shown in Fig. 2. After a short synthesis duration (3 min), the powder color obviously changes from white to black (Fig. 1), indicating that the graphene is completely deposited on the TiO_2 NPs.

Point discharge through the conductive SiO_2/Si slices occurs around the tips in the microwave oven system. Because of the continuous and acute partial discharge, the temperature quickly reaches 600~700 °C in few minutes. When the carbon precursor (methane) is introduced into the oven system, the discharge and high temperature cause the decomposition of methane into highly reactive species (·CH_x and atom H) which can generate graphene nanosheets in the pure gas phase and be absorbed to the TiO_2 NP surface, forming the graphene nanosheets on the gas-solid interface. Compared with the growth of vertical graphene via plasmas enhanced CVD (PECVD), the graphene growth via microwave also presents the transition of growth direction from parallel to vertical. In the microwave oven system, the induction of the electromagnetic field brings a strong effect on the growth orientation of the vertical graphene nanosheets[6].

2.2 Characterization of G/TiO_2 nanocomposites

The average diameter of the commercial TiO_2 NP is about 25 nm. The high resolution TEM (HRTEM) image of TiO_2 NP (Fig.3a) shows that the *d*-spacing of the distinct lattice fringes is about 0.35 nm, which is consistent with the interplanar distance of (101) planes of anatase TiO_2 phase[7]. As shown in Fig.3b, HRTEM image of G/TiO_2 nanocomposites shows that the interplanar distance of (101) planes is also about 0.35 nm, indicating that the TiO_2 phase remains the anatase structure. It can be seen form the insets in Fig.3b that the layer number of
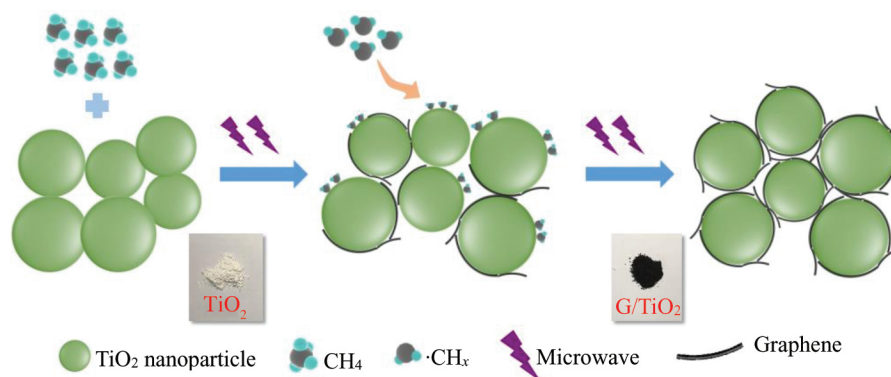

Fig.1　Schematic diagram of synthesis of G/TiO_2 nanocomposites by modified household microwave oven system
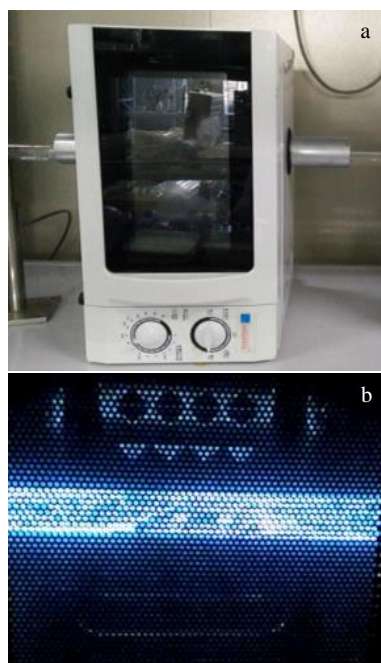
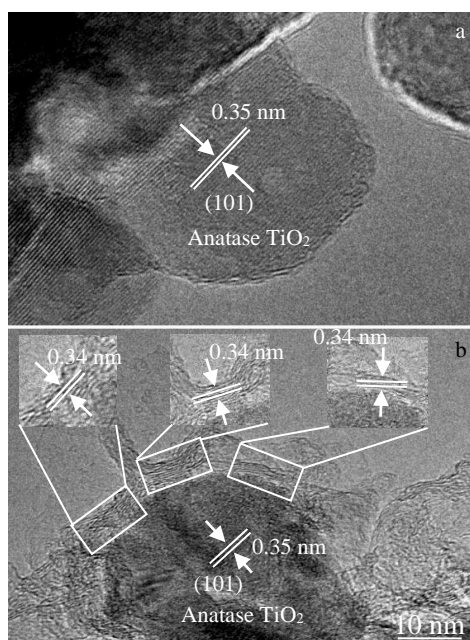Fig.2 Appearances of modified household microwave oven (a) and continuous bright flash during synthesis (b)

Fig.3 HRTEM images of anatase TiO$_2$ NPs (a) and G/TiO$_2$ nanocomposites (b)

graphene nanosheet is 5~7. The graphene nanosheet size is about 50 nm. The interlayer spacing of about 0.34 nm can also be observed in the graphene nanosheets.

The phase structure of G/TiO$_2$ nanocomposites can be characterized by Raman spectra. Fig.4a shows that the three peaks at 377, 499, and 618 cm^{-1} correspond to the B$_{1g}$, A$_{1g}$, and E$_g$ active modes of anatase TiO$_2$, respectively. When the
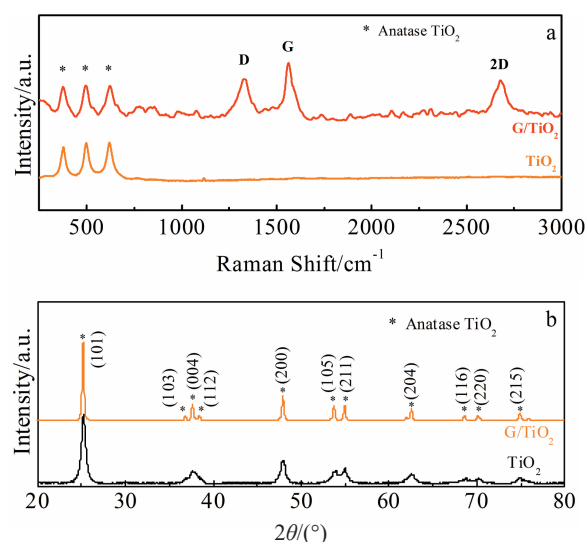

Fig.4 Raman spectra (a) and XRD patterns (b) of anatase TiO$_2$ NPs and G/TiO$_2$ nanocomposites

anatase TiO$_2$ NPs are calcined at high temperature for a long time, the lattice oxygen will be released and the phase structure will be destroyed. After the growth process, these three peaks of G/TiO$_2$ nanocomposites do not shift, compared with those of the anatase TiO$_2$. The phase structure does not change during the fast growth process. Additionally, the broad Raman bands at 1345 and 1580 cm^{-1} are attributed to the A$_{1g}$ active mode of disordered carbon (D-peak) and the E$_{2g}$ active mode of graphitic carbon (G-peak), respectively. The D-peak presents as the defects due to the edges of the graphene nanosheets[8]. Therefore, the relative intensity of D-peak to G-peak (I_D/I_G) is used to roughly estimate the defect degree. The I_D/I_G ratio of G/TiO$_2$ nanocomposites is 0.65, which is smaller than that of rGO and some CVD-coated graphene, indicating a relatively low defect degree of graphene nanosheets[9]. The high graphitization degree can improve the electrical conductivity of G/TiO$_2$ nanocomposites.

As shown in Fig.4b, these diffraction peaks of TiO$_2$ NPs are in good agreement with those of the anatase TiO$_2$ phase (JCPDS, No. 21-1272). After the growth process in the microwave oven system, XRD pattern of G/TiO$_2$ nanocomposites still presents the characteristic of anatase TiO$_2$ phase, and some diffraction peaks (36°<2θ<39°) become more obvious. These results indicate that there is no phase transformation from anatase to rutile. However, the main diffraction peak at 2θ=25.2° originating from the (101) plane of anatase TiO$_2$ and that of graphene at 2θ=26.2° overlap. Therefore, XRD pattern of G/TiO$_2$ nanocomposites does not show the characteristic peak of graphene.

XPS spectrum in Fig.5a verifies the presence of C, Ti, and O elements. The high resolution XPS spectra (Fig.5b) for Ti 2p of G/TiO$_2$ nanocomposites can be regarded as two components at 458.9 and 464.6 eV, namely Ti 2p$_{3/2}$ subpeak and Ti 2p$_{1/2}$ subpeak, respectively[10]. A spin-energy separation of 5.7 eV in Ti 2p shows the TiO$_2$ characteristic. Four

components of C 1s spectra (Fig. 5c) at 284.18, 285.41, 288.29, and 291.48 eV correspond to C-C, C-H, C-O, and C=O bonds, respectively[11]. These results indicate that the sp^2 carbon is the main structure and few defects can be observed in the graphene nanosheets. Besides, the surface elements and chemical bonding states of G/TiO_2 nanocomposites are in good agreement with the Raman, XRD, and XPS results.

The energy dispersive spectroscopic (EDS) mapping was used to characterize the element distribution. Fig. 5d shows TEM image of G/TiO_2 nanocomposites. The uniform distribution of C (Fig.5e), Ti (Fig.5f), and O (Fig.5g) elements can be clearly observed. These results confirm that the graphene nanosheets are uniformly composited with TiO_2 NPs.

2.3 Electrochemical characterization of G/TiO_2 nanocomposites as anode materials

The electrochemical performance of both the G/TiO_2 nanocomposites and TiO_2 NPs as anode materials was evaluated through lithium batteries in the voltage range of 1~3 V in half-cell configuration at room temperature (Fig. 6). Generally, lithium insertion/extraction in anatase TiO_2 occurs reversibly based on the conversion reaction[12], as follows:

$$TiO_2+xLi^++xe^-=Li_xTiO_2 \ (x{\leq}1) \tag{1}$$
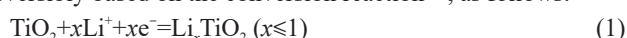
The anatase TiO_2 has a body-centered tetragonal crystal structure, and the theoretical capacity is 335 mAh·g⁻¹ under the cycle condition of 1.0 V vs. Li⁺/Li. As the crystal structure of anatase TiO_2 changes, the capacity and cycle stability can be sharply reduced. Fig.7 shows the cyclic voltammetry (CV) curves of the first five cycles of the G/TiO_2 nanocomposites at a scan rate of 0.05 mV·s⁻¹. The half-cell shows an open circuit voltage (OCV) of about 2.49 V vs. Li⁺/Li. In the insertion of lithium ions into TiO_2 crystal lattice during the first discharging, the valence state of titanium changes from Ti⁴⁺ to Ti³⁺. During the first cathodic cycle, the sharp peak at a potential of about 1.69 V vs. Li⁺/Li is mainly attributed to the Li insertion and the reduction from Ti⁴⁺ to Ti³⁺. During the first anodic cycle, the sharp peak at a potential of about 2.06 V vs. Li⁺/Li corresponds to the Li extraction and the oxidation from Ti³⁺ to Ti⁴⁺. The possible structure rearrangement of TiO_2 crystal lattice leads to slight deviations in the peak positions, which can be noted in the subsequent four cycles. Compared with the CV curves of G/TiO_2 nanocomposites, those of TiO_2 NPs show the similar sharp peaks at about 1.68 and about 2.06 V vs. Li⁺/Li during cathodic and anodic cycles, respectively. However, the low intensity and obvious position deviations of the two peaks can be observed. The cathodic and anodic cycles results indicate the excellent reversibility and extended two-phase reaction in the G/TiO_2 nanocomposites.

As Li-ions are inserted into the TiO_2 matrix during the discharging, the lattice phase changes from tetragonal to orthorhombic ($Li_{0.5}TiO_2$) phase due to the loss of symmetry along the y direction[13]. The initial discharge capacity of 225 mAh·g⁻¹ at a current density of 33 mA·g⁻¹ corresponds to the insertion of 0.67 mol Li per formula unit (the theoretical capacity of 335 mAh·g⁻¹ corresponds to 1 mol Li). The 1.76 V vs. Li⁺/Li of discharging plateau and 1.9 V vs. Li⁺/Li of charging plateau correspond to the Li insertion/extraction between the tetragonal and orthorhombic ($Li_{0.5}TiO_2$) phases. This two-phase region possibly originates from the interfacial
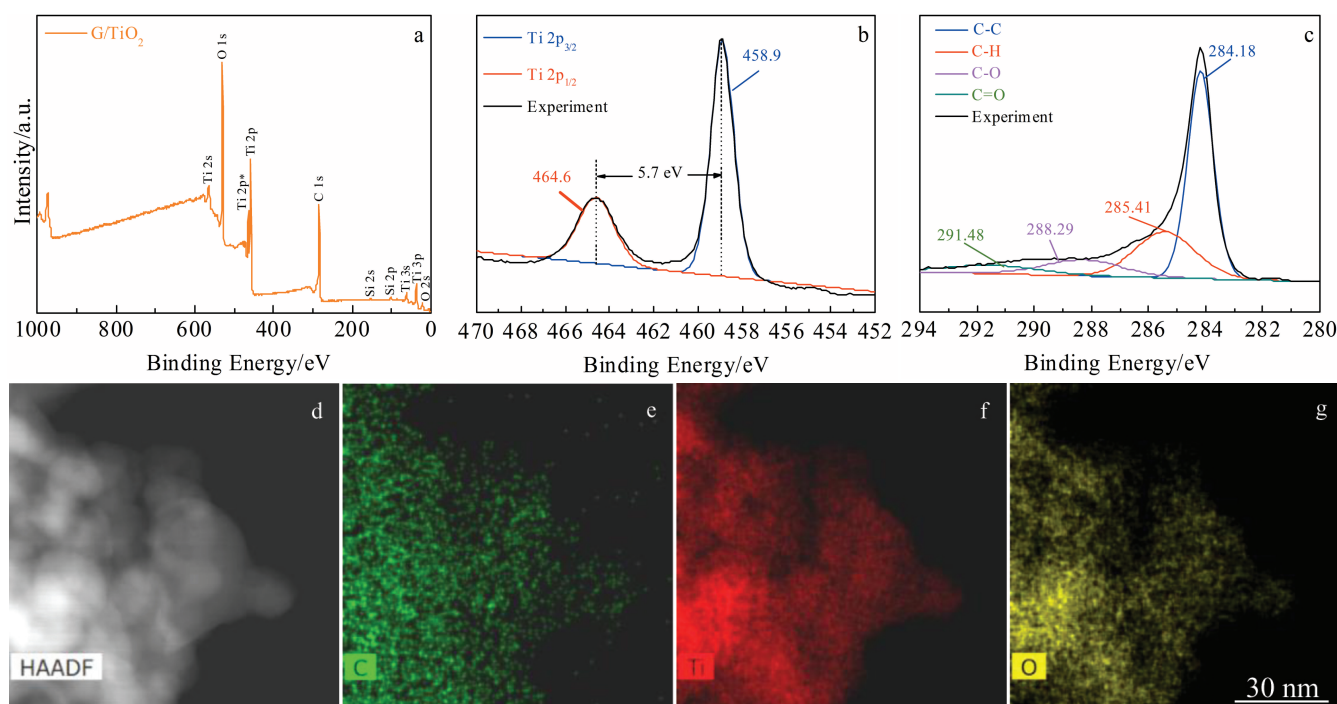

Fig.5　XPS spectra of G/TiO_2 (a), Ti (b), and C (c) in G/TiO_2 nanocomposites; TEM image (d) and corresponding C (e), Ti (f), and O (g) element distributions of G/TiO_2 nanocomposites
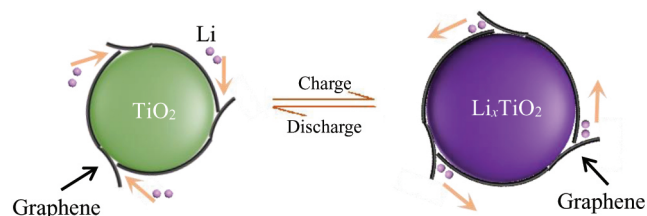
Fig.6   Schematic diagram of G/TiO$_2$ nanocomposites as anode materials during charging-discharging
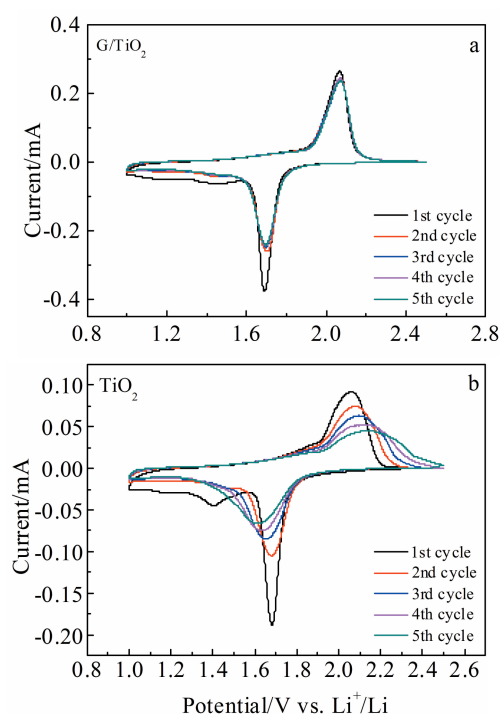

Fig.7   CV curves of G/TiO$_2$ nanocomposites (a) and TiO$_2$ NPs (b) as electrodes in the first five cycles at scan rate of 0.05 mV·s^{-1}

lithium storage. Meanwhile, based on the two-phase reaction mechanism, Li-ion is inserted into the TiO$_2$ matrix via the presence of plateau region during the charging/discharging process. Some similar two-phase regions were reported in other graphene/TiO$_2$ composites[14,15].

The first discharging (Li$^+$ insertion) and charging (Li$^+$ extraction) curves of G/TiO$_2$ nanocomposites as an anode material at a rate of 1 C is shown in Fig.8a. The discharge and charge capacities of the first cycle of G/TiO$_2$ nanocomposites are 146.1 and 161.9 mAh·g^{-1}, respectively, which is 90.2% of the initial Coulombic efficiency. The Coulombic efficiency can reach 99% after a few cycles. The discharge capacity of G/TiO$_2$ anode is 95 mAh·g^{-1} after 120 cycles, which is about 65% of the initial capacity. The capacity fading is estimated as 0.308 mAh·g^{-1} per cycle, except the first 10 cycles. The discharge and charge capacities of the first cycle of TiO$_2$ NPs are 188.6 and 252.1 mAh·g^{-1}, respectively, which is 74.8% of the initial coulombic efficiency. The coulombic efficiency obviously fluctuates in the subsequent cycles. After 120

cycles, the discharge capacity is only 27.2 mAh·g^{-1}, which is about 14% of the initial capacity. Thus, the as-prepared G/TiO$_2$ nanocomposite electrode shows a two-fold increase of capacity with good cycling stability under the condition of 1 C (170 mA·g^{-1}), compared with the anatase TiO$_2$ NPs. The formation of solid electrolyte interface (SEI) film on the electrode surface, some side reactions between Li$^+$ and defects in the graphene nanosheets, and the loss of symmetry during phase transition are the main reasons for the large irreversible capacity loss[9]. Compared with the results of TiO$_2$ NPs as anode material, better cycling stability and higher specific capacity of G/TiO$_2$ nanocomposite electrode are obtained, which indicates a strong synergistic effect between the graphene nanosheets and TiO$_2$ components, thereby improving the interface conductivity and restricting the increase in unit cell volume[16].

The specific capacity of electrode was also measured at different charging/discharging rates from 0.5 C to 5 C (Fig. 8b). The specific capacity of G/TiO$_2$ nanocomposite electrode is 135, 125, 118, 105, and 95 mAh·g^{-1}, whereas that of TiO$_2$ NPs is 160, 126, 40, 18, and 10 mAh·g^{-1} at charging/discharging rate of 0.5, 1, 2, 3, and 5 C, respectively. The specific capacity of G/TiO$_2$ nanocomposites is increased at the higher charging/discharging rates (2~5 C). The TiO$_2$ NP electrode cannot maintain the initial specific capacity at high charging/discharging rate of 5 C. On the one hand, the specific
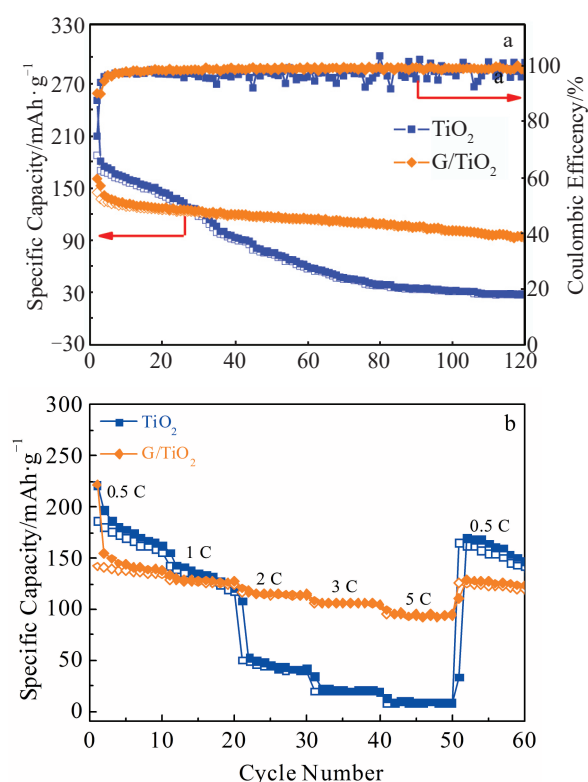

Fig.8   Cycling performance of TiO$_2$ NPs and G/TiO$_2$ nanocomposites at charging/discharging rate of 1 C (a); specific capacity of TiO$_2$ NPs and G/TiO$_2$ nanocomposites at different charging/discharging rates (b)

capacity of G/TiO$_2$ nanocomposite is 10 and 3 times higher than that of TiO$_2$ NPs at the charging/discharging rate of 5 and 2 C, respectively. On the other hand, as the charging/discharging rate increases to 2 C, the specific capacities of TiO$_2$ NPs and G/TiO$_2$ nanocomposites maintain about 32% and 85% of those at 1 C, respectively. Furthermore, as the charging/discharging rate is decreased to 0.5 C again, the G/TiO$_2$ nanocomposite electrode can resume its specific capacity of about 135 mAh·g^{-1} after 50 cycles, indicating that the G/TiO$_2$ nanocomposite electrode has good rate capability and cycling stability.

The decrease in specific capacity is ascribed to the less participation of active material in the charging-discharging reaction accompanied by the increase in charge-discharge rate[17]. It should be noted that the specific capacities of G/TiO$_2$ nanocomposite electrode are lower than that of TiO$_2$ NP electrode at relatively low charging/discharging rate of 0.5 C, regardless of the initial cycles or the final cycles. The possible main reason is that the in-situ synthesis of graphene nanosheets uniformly encapsulates the surface of TiO$_2$ NPs, resulting in the relatively obvious hindrance to transfer the Li-ion into TiO$_2$ matrix at low current density. With increasing the current density, the hindrance effect of graphene becomes less obvious at G/TiO$_2$ cell.

3 Conclusions

1) In the modified microwave oven system, the graphene nanosheets can be uniformly distributed on the surface of anatase TiO$_2$ nanoparticles in a few minutes (the minimum duration is 3 min).

2) The anatase crystal structure of TiO$_2$ remains after the synthesis process, which is attributed to the low production temperature (600~700 °C) and short production period.

3) The excellent electrical conductivity of graphene can improve the Li-ion diffusion and electron transport, and decrease the contact resistance at the interface of electrode/electrolyte.

4) The as-prepared graphene/TiO$_2$ nanocomposite electrode shows a two-fold increase of capacity with good cycling stability under the condition of 1 C (170 mA·g^{-1}), compared with the anatase TiO$_2$ nanoparticles.

References

1 Geim A K. *Science*[J], 2009, 324(5934): 1530

2 Billups W E, Singh N, Mital G *et al. ACS Nano*[J], 2011, 5(6): 4345

3 Wang Weiwei, Wang Wenfang, Chen Xiaoli *et al. Rare Metal Materials and Engineering*[J], 2015, 44(9): 2138

4 Wang H, Joshua T R, Dai H *et al. Journal of the American Chemical Society*[J], 2010, 132(10): 3270

5 Shi Liurong, Pang Chunlei, Chen Shulin *et al. JPC Bulletin on Iron & Steel*[J], 2017, 17(6): 3681

6 Ci Haina, Ren Huaying, Qi Yue *et al. Nano Research*[J], 2018, 11(6): 3106

7 Zhao Dongyuan, Wang Guoxiu, Shen Dengke *et al. Journal of the American Chemical Society*[J], 2015, 137(40): 13 161

8 Jiang D, Novoselov K S, Casiraghi C *et al. Physical Review Letters*[J], 2006, 97(18): 1 874 011

9 Xie Keyu, Li Xu, Wei Bingqing *et al. ACS Nano*[J], 2016, 10(6): 6227

10 Sodergren S, Siegbahn H, Rensmo H *et al. The Journal of Physical Chemistry B*[J], 1997, 101(16): 3087

11 Saito Yusuke, Fukushima Takanori, Matsumoto Michio *et al. Nature Chemistry*[J], 2015, 7(9): 730

12 Patoux S, Masquelier C. *Chemistry of Materials*[J], 2002, 14(12): 5057

13 Wagemaker M, Kentgens A P M, Mulder F M. *Nature*[J], 2002, 418(6896): 397

14 Wang Donghai, Choi Daiwon, Li Juan *et al. ACS Nano*[J], 2009, 3(4): 907

15 Shen Laifa, Zhang Xiaogang, Li Hongsen *et al. Journal of Physical Chemistry Letters*[J], 2011, 2(24): 3096

16 Zhang Xiang, Kumar Palaniswamy Suresh, Aravindan Vanchiappan *et al. Journal of Physical Chemistry C*[J], 2012, 116(28): 14 780

17 Zaghib K, Mauger A, Goodenough J B *et al. Journal of Power Sources*[J], 2009, 194(2): 588

微波原位制备作为锂离子电池电极材料的石墨烯/TiO₂纳米复合物

杨良伟，陈昊然，金　鑫，刘　伟，于新民，刘俊鹏，宋环君，李晓东，于　艺，王　鹏，张宝鹏
(航天特种材料及工艺技术研究所，北京　100074)

摘　要：通过改造的家用微波炉，实现了原位高效制备石墨烯/TiO₂纳米复合物。结果表明：微波辅助法能够在商用锐钛矿型 TiO₂ 纳米颗粒表面均匀制备石墨烯纳米片，通过 SiO₂/Si 的剧烈电晕放电，其制备时间仅需数分钟（最短 3 min）。石墨烯纳米片的尺寸大约为 50 nm 且缺陷很少。TiO₂ 晶体结构仍为锐钛矿型，主要归功于极短的制备周期和较低的反应温度（600~700 ℃）。石墨烯具有优异的电导率，可以提升锂离子扩散速率、提高电子传输速率并降低接触电阻。在 1 C（170 mA·g⁻¹）条件下石墨烯/TiO₂纳米复合物的电池放电比容量提高了 2 倍。与商业化锐钛矿型 TiO₂ 纳米颗粒相比，在 1 C 到 5 C 的不同充放电倍率下，石墨烯/TiO₂纳米复合物的比容量差距显著扩大。
关键词：石墨烯/TiO₂纳米复合物；微波辅助；电晕放电；原位制备；锂离子电池